Available online at www.sciencedirect.com
SCIENCE DIRECT
Journal of Catalysis 238 (2006) 468–476
JOURNAL OF CATALYSIS
www.elsevier.com/locate/jcat

Preparation and characterization of carbon-supported PtRuIr catalyst with excellent CO-tolerant performance for proton-exchange membrane fuel cells

Yongmin Liang [a,b], Huamin Zhang [a,*], Hexiang Zhong [a,b], Xiaobing Zhu [a,b], Zhiqun Tian [a], Dongyan Xu [a], Baolian Yi [a]

[a] *Proton Exchange Membrane Fuel Cell Key Materials and Technology Laboratory, Dalian Institute of Chemical Physics, Chinese Academy of Sciences, PO box 110, Dalian 116023, China*

[b] *Graduate School of the Chinese Academy of Sciences, Beijing, 100039, China*

Received 30 September 2005; revised 5 January 2006; accepted 6 January 2006

Abstract

A PtRuIr/C catalyst was prepared using a microwave-irradiated polyol plus annealing (MIPA) synthesis strategy and characterized by a series of techniques. The results are discussed in comparison with those for PtRu/C catalyst prepared in the same way; they show insignificant difference in particle morphology, particle size, size distribution, phase structure, and compositional homogeneity. CO stripping voltammetry and single-proton exchange membrane fuel cell tests reveal that including Ir in the PtRu system results in an excellent CO_{ads} electro-oxidation activity. Based on exploration of the structure–performance relationship, a speculative mechanism for the superior performance of the PtRuIr/C catalyst is proposed that suggests that the enhanced performance is attributed mainly to the interaction between RuO_2 and IrO_2, leading to facile oxidation of CO_{ads} on active metal sites at a lower potential relative to the PtRu/C analogue.

Keywords: Proton exchange membrane fuel cells; Anode catalyst; Carbon monoxide oxidation; Microwave irradiation; Polyol; PtRuIr

1. Introduction

Hydrogen (H_2) is the ideal fuel for proton exchange membrane (PEM) fuel cells and typically produced via steam reforming or partial oxidation of methanol or other hydrocarbons [1,2]. Platinum supported on high-surface area carbon black has proven to be the most active catalyst for hydrogen oxidation reaction (HOR) occurring at the anode of the PEM fuel cells [3,4]. Unfortunately, however, carbon monoxide (CO) is a byproduct of these H_2 production processes, and even a few ppm of CO contained in the H_2 stream can severely poison the platinum catalyst [1–7]. The CO poisoning problem leads to significantly decreased output power and energy utilization efficiency, and currently remains one of the challenges hindering the commercialization of PEM fuel cells [1].

Efforts to mitigate CO poisoning have been concentrated on the addition of cocatalysts, such as Ru [1–17], Mo [18,19], Sn [19], W [19,20], Nb [21], and Ni [22–25], to platinum. Other systems (e.g., PdAu [26]) have also been studied as CO-tolerant catalysts, and considerable advances have been made. Of many possibilities, the binary PtRu system is now recognized as the most promising candidate [1,3,7,8].

There are two proposed mechanisms for the improved CO-tolerance of the state-of-the-art PtRu catalyst [2,4,12]. One is promoted mechanism, according to which the oxophilic ruthenium in the PtRu catalyst dissociates water into OH and H at a lower potential than that on platinum. The CO chemisorbed on the platinum sites can then be oxidized by the nearby OH species. The other is an intrinsic mechanism by which the electronic structure of platinum is modified by forming an alloy with Ru. This results in the weakening of the carbon monoxide adsorption on platinum. Both mechanisms imply that the particle size and composition should be delicately controlled; that is, Pt and the promoting metals should intimately contact at atomic scale or form alloy clusters with compositional ho-

* Corresponding author. Fax: +86 411 84665057.
E-mail address: zhanghm@dicp.ac.cn (H. Zhang).

0021-9517/$ – see front matter
doi:10.1016/j.jcat.2006.01.005

mogeneity, and the nanoparticles should have a narrow size distribution [3,10,11]. From the standpoint of the commercialization of PEM fuel cells, the modified performance by carbon-supported PtRu nanocomposites is still not enough, and more active catalysts for HOR in the presence of CO are critically needed for a practical application of this technology [1].

In this work, a carbon-supported PtRuIr nanocomposite is prepared via the microwave-irradiated polyol plus annealing (MIPA) synthesis strategy. The addition of iridium to the PtRu system is based mainly on the consideration that iridium dioxide (IrO_2) has a good activity toward oxygen evolution reaction [27–30]. Inclusion of iridium may thus promote the oxidation of the CO_{ads} species on the active metal sites.

In the MIPA process, the metal salts are reduced by ethylene glycol with microwave irradiation as the heating source. The process combines the advantages of high dielectric loss (dielectric constant, 41.4 at 20 °C [31]) of ethylene glycol and the fast and homogeneous heating property of microwave irradiation and thus can result in a rapid reaction rate, small particle size, and narrow size distribution. The method was first applied by Komarneni et al. [32] to prepare nanosized metallic particles and has recently attracted great attention in the field of metal nanoparticle synthesis [10,33–36]. Reductive annealing of the nanocomposite aims to promote the interaction of the metals [3,6]. Duplicate experiments have confirmed that our PtRuIr/C catalyst has a very high activity for CO_{ads} electrooxidation, even higher than that of the commercial PtRu/C catalyst. A speculative mechanism for the superior performance of the PtRuIr/C catalyst is proposed on the basis of exploration of the structure–performance relationship.

2. Experimental

2.1. Catalyst preparation

The synthesis was carried out with the aid of a domestic microwave oven (LG WD700, 700 W, 2450 MHz). Vulcan XC-72R carbon black (Cabot Corp., $S_{BET} = 250\ m^2/g$) was used as the support. The catalyst having 40 wt% metal and Pt:Ru:Ir atomic ratio of 1:1:1 was typically prepared as follows: 200 mg of Vulcan XC-72R carbon black was added in 120 ml of ethylene glycol and stirred vigorously to obtain a slurry. Then solutions of 2.48 ml of 0.1517 M hexachloroplatinic acid in ethylene glycol, 10.27 ml of 0.0366 M ruthenium(III) chloride in ethylene glycol, and 1.5 ml of 0.1821 M chloroiridic acid in ethylene glycol were mixed and subsequently added to the slurry. The suspension was stirred for 30 min and ultrasonicated for another 30 min, followed by the addition of a 2.5 M ethylene glycol solution of sodium hydroxide to increase the pH to >10. The suspension was exposed to microwave irradiation in a 90 s on–10 s off–60 s on heating strategy, then cooled to room temperature. Hydrochloric acid (3 M) was added to lower the pH to <1, to induce sedimentation of the as-synthesized PtRuIr nanocomposite. The product was recovered by centrifugation and washing with ethanol for several times and dried in a vacuum oven at 80 °C for 8 h. The dry powder was then reductively annealed under flowing nitrogen (5% H_2/N_2, 500 °C, 4 h). The catalyst thus obtained is denoted as DICP PtRuIr/C. For comparison, Vulcan XC-72R-supported PtRu nanocomposite with 40 wt% metal and a Pt:Ru atomic ratio of 1:1 and Vulcan XC-72R-supported Ir catalyst with 40 wt% metal were also prepared in the same way and are denoted as DICP PtRu/C and DICP Ir/C, respectively.

2.2. Catalyst characterization and evaluation

Transmission electron microscopy (TEM) images were recorded on a JEOL JEM-2000EX microscope operated at 100 kV. Samples for TEM measurements were prepared by ultrasonically suspending catalyst powder in ethanol and placing a drop of the suspension to a holey amorphous carbon film on a Cu grid. Particle size distributions for the catalysts were obtained by manually measuring 200 particles from the bright-field micrographs. The mean particle diameter d_m was calculated by the following formula [37]:

$$d_m = \sum_i n_i d_i \Big/ \sum_i n_i,$$

where n_i is the number of particles with diameter d_i.

Inductively coupled plasma–atomic emission spectroscopy (ICP-AES) analyses of the DICP PtRuIr/C and DICP PtRu/C catalysts were conducted to determine bulk contents of the metals. Energy-dispersive spectroscopy (EDS) analyses were performed with a JSM-5600LV analyzer working at accelerating voltage of 200 kV.

X-ray diffraction (XRD) scans were conducted on a PANalytical powder diffractometer (Philips X'Pert PRO) using Ni-filtered Cu-K_α radiation ($\lambda = 1.54056$ Å). The angle extended from 20° to 95° and varied with a step size of 0.017°, accumulating data for 8.255 s per step. The (220) peaks of Pt fcc reflection patterns were fitted to Gaussian line shapes on a linear background. Scherrer's formula and Bragg's equation [13,34] were then applied to obtain the average particle sizes and lattice parameters, respectively.

XPS spectra were obtained using a VG ESCALAB MK2 spectrometer equipped with Al-K_α source (1486.6 eV, 12.5 kV, 250 W). The base pressure of the system was 2×10^{-8} Pa, and the measurements were carried out at 2×10^{-7}–1×10^{-6} Pa. For each catalyst, a survey spectrum was collected before high-resolution spectra were recorded. Deconvolutions of the XPS spectra were carried out using software XPS Peak 4.1. Relative concentrations of the surface species are equal to the corresponding deconvoluted peak areas divided by the total XPS signal area extracted from the experimental XPS core level regions of either Pt4f, Ru3p, or Ir4f.

An EG & G potentiostat/galvanostat model 263A (Princeton Applied Research) and a conventional three-electrode system were used to conduct CO stripping voltammetry experiments on the DICP PtRuIr/C, DICP PtRu/C, DCIP Ir/C, and the commercially available E-TEK 40 wt% PtRu/C (identified as E-TEK PtRu/C) catalysts at 25 °C in 0.5 M H_2SO_4. The working electrode was prepared as follows: 5 mg of catalyst was mixed with 1 ml of ethanol and 50 μl of 5.4% Nafion solution (Aldrich). The mixture was sonicated for 30 min to obtain an ink-like

slurry. Then 25 μl of the slurry was applied to the surface of the vitreous carbon electrode to form a thin layer about ca. 0.196 cm^2 in geometric area. A saturated calomel electrode (SCE), which has a potential of 0.242 V versus the reversible hydrogen electrode (RHE) and a large surface area platinum foil, were used as the reference electrode (separated by an electrolyte bridge) and the counter electrode, respectively. Before each measurement, the solution was purged with high-purity nitrogen for 30 min. Pure CO was then bubbled for 30 min with the potential held at −0.224 versus SCE to allow complete adsorption of CO onto the active catalytic sites. This CO adsorption potential is typical for application in a PEM fuel cell [21]. After each adsorption, CO remained in the solution was removed by bubbling high-purity nitrogen for 30 min. Two cyclic voltammetries were collected between −0.242 and 0.96 V versus SCE with a scan rate of 20 mV/s. The first potential sweep was conducted to electro-oxidize the irreversibly adsorbed CO and the second sweep to verify the complete oxidation of the adsorbed species. All potentials throughout this paper were referred to SCE. The amount of CO_{ads} was estimated by integration of the CO_{ads} stripping peak, corrected for the electric double-layer capacitance. The electrochemically active surfaces of the catalysts were obtained as described previously [9] assuming a monolayer of linearly adsorbed CO and the charge density required for oxidation as 0.42 mC/cm^2.

The catalytic activity for HOR in the presence of 100 ppm CO of DICP PtRuIr/C and DICP PtRu/C were evaluated as the single PEM fuel cell anode catalysts and compared with that for the E-TEK PtRu/C catalyst. For all three anodes, the catalyst powder (metal + carbon support) was maintained at ∼1 mg/cm^2 to ensure the same thickness, and hence the same electric resistance, of the catalyst layers. The anode metal loadings were kept at ca. 0.4 mg/cm^2. In all cases, the cathodes adopted the commercial 50 wt% Pt/C catalyst (Johnson Matthey) with platinum loading of 0.37 mg/cm^2, with Nafion 112 (H^+ form, Du Pont) used as the membrane. Fabrication of the electrodes and membrane electrode assemblies (MEAs) followed the process reported by Ticianelli et al. [17]. The MEAs had an active area of 5 cm^2. In all cases, oxygen instead of air was used as the oxidant to minimize polarization at the cathode, thus making the difference of the anode catalysts more apparent. The fuel gas (100 ppm CO/H_2) and oxygen were humidified at temperatures of 90 and 85 °C, respectively, before feeding into the cells. The cells were operated at 80 °C and 0.2 MPa. The inlet and outlet gases of the anodes of the fuel cells were analyzed by gas chromatography (Shimadzu, GC-14A, FID), and mass balance calculation was carried out to determine the conversion of carbon monoxide in the hydrogen-rich stream to carbon dioxide.

3. Results and discussion

It is well known that metal particle morphology, particle size, and size distribution strongly affect catalyst properties [34]. With this in mind, we first carried out TEM examination on the as-prepared DICP PtRuIr/C and DICP PtRu/C catalysts to study the effect of including Ir in the PtRu system on particle size and size distribution. The typical bright-field TEM images of the DICP PtRuIr/C and DICP PtRu/C catalysts are shown in Figs. 1a and 1b, respectively. It can be seen that the spherical metal particles of the two catalysts are uniformly dispersed on the carbon supports, with some aggregates observed in DICP PtRu/C. Figs. 2a and 2b show the histograms of the particle size distributions. The particle size for the DICP PtRuIr/C catalyst ranges between 1 and 5 nm, with a mean di-

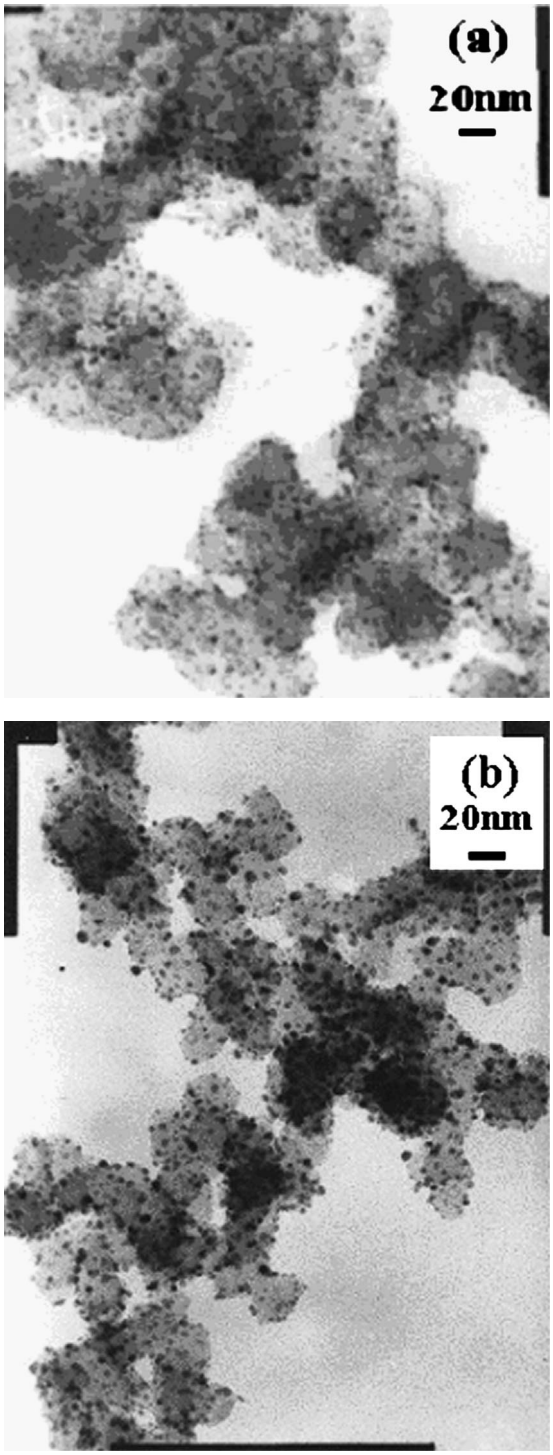

Fig. 1. Bright-field TEM images of (a) DICP PtRuIr/C and (b) DICP PtRu/C catalysts.

ameter d_m of 2.9 nm. For the DICP PtRu/C catalyst, the mean particle diameter is 3.2 nm and the size distribution is 1–7 nm. The small particle size and the homogeneous size distribution of both catalysts are ascribed to the rapid reduction of the metal salts and easy nucleation of the metal particles in ethylene glycol facilitated by microwave irradiation [32,34,36,38]. The increased dispersion of the DICP PtRuIr/C catalyst with respect to that of the DICP PtRu/C catalyst may be attributed to the enhanced agglomeration resistance associated with iridium oxides [39].

Most researchers now agree that PtRu nanoparticles with an average diameter of 2–4 nm exhibit the best electrocatalytic activity for application in PEM fuel cells [33,38,40]. Although it is not yet clear whether this size range is also an optimum value for the ternary PtRuIr nanocomposite, it is apparent that the addition of iridium has a rather small effect on particle shape, particle size, and size distribution.

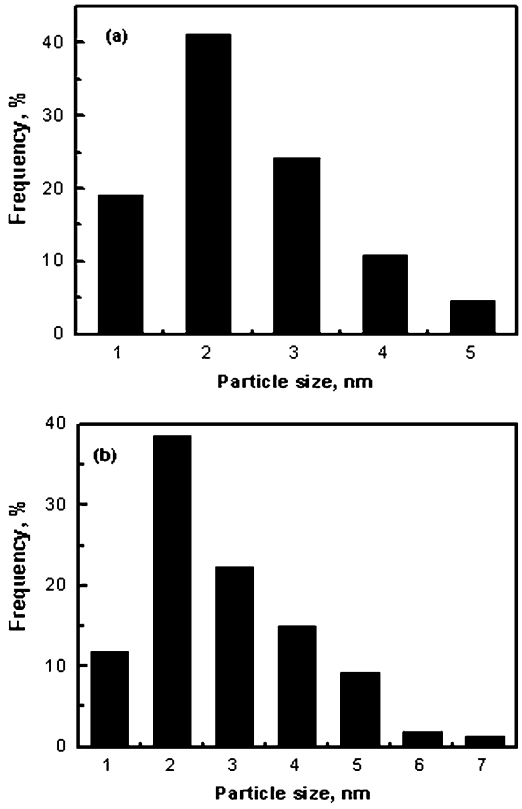

Fig. 2. Histograms of metal particles diameters for (a) DICP PtRuIr/C and (b) DICP PtRu/C catalysts.

Table 1
Metal content in DICP PtRuIr/C, DICP PtRu/C and DICP Ir/C catalysts

Catalyst sample	Metal nominal content[a] (wt%)			Metal actual content[b] (wt%)		
	Pt	Ru	Ir	Pt	Ru	Ir
DICP PtRuIr/C	15.98	8.28	15.74	13.54	5.13	14.24
DICP PtRu/C	26.3	13.7	–	24.02	10.41	–
DICP Ir/C	–	–	40	–	–	37.4

[a] As calculated from metal content of 40 wt% and atomic ratio of 1:1:1 for Pt:Ru:Ir or of 1:1 for Pt:Ru.
[b] As determined from ICP-AES analyses.

ICP-AES was conducted to determine the bulk metal content in the DICP PtRuIr/C and DICP PtRu/C catalysts. The results, presented in Table 1, show that the content of Pt and/or Ir in both catalysts is relatively close to their nominal values; however, Ru content is comparatively lower than their nominal values. Two factors may be responsible for the low Ru content in the two samples. Incineration treatment of the samples before the elemental analysis is performed may result in loss of volatile ruthenium oxides. Moreover, the relatively weaker interaction of Ru^{3+} compared with those for $PtCl_6^{2-}$ and $IrCl_6^{2-}$, with the surface groups of the support could contribute to less adsorption of Ru^{3+} on the support and thus the low Ru content [11]. The Pt:Ru:Ir and Pt:Ru atomic ratios, as calculated from the measured contents, are 1.37:1:1.46 and 1.2:1, respectively.

The on-particle EDS analysis was used to monitor the compositional homogeneity of individual particles. It should be noted that variation of the composition for the individual particles is relatively small. The Pt:Ru:Ir and Pt:Ru atomic ratios measured by EDS turn out to be 1.07:1:1.23, and 1.13:1, respectively, which are in good agreement with the bulk values.

XRD analyses were performed to obtain structural information of the catalysts. Fig. 3 shows the XRD patterns of the DICP PtRuIr/C and DICP PtRu/C catalysts. As it is shown in the figure, both of the nanocomposites exhibit only characteristic diffraction peaks (marked in the figure) of the fcc platinum [13,16,33]. No diffraction peaks, which would be attributed to pure ruthenium and iridium or their oxides/hydroxides, appear in the XRD patterns. The diffraction peaks of the DICP PtRuIr/C catalyst are found to shift positively with respect to those of the DICP PtRu/C analogue. The average crystallite sizes for the DICP PtRu/C and DICP PtRuIr/C catalysts, calculated by Scherrer's formula [13,34], are 3.0 and 3.3 nm, respectively, which are very close to those obtained by TEM. Bragg's equation [13] is used to obtain the lattice parameters of 3.834 Å for the DICP PtRuIr/C catalyst and 3.886 Å for the DICP PtRu/C catalyst. A comparison with the values of 3.916 Å for carbon-supported platinum and 3.860 Å for bulk PtRu alloy may support the idea that the metals form alloy [3,13]. However, for the moment, we would be cautious in drawing the conclusion of alloy formation in our ternary PtRuIr/C catalyst, because according to our experience, the small size and the support may cause distortion of the lattice planes, and obtaining direct proof

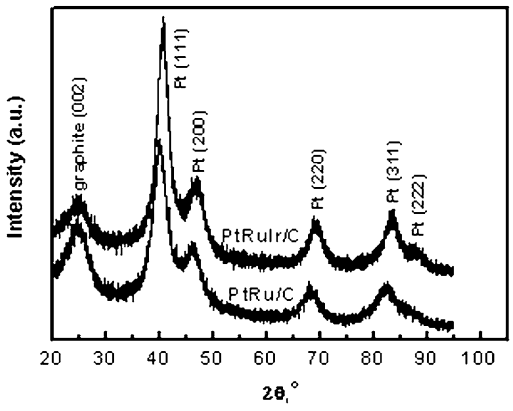

Fig. 3. Powder XRD patterns of DICP PtRuIr/C and DICP PtRu/C catalysts.

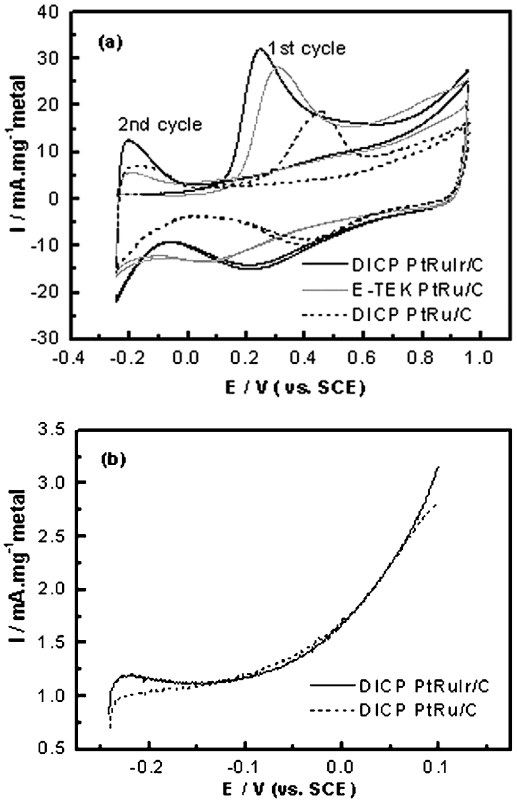

Fig. 4. (a) CO-stripping voltammograms of DICP PtRuIr/C, DICP PtRu/C and E-TEK PtRu/C catalysts in 0.5 M H_2SO_4 at 25 °C. (b) Voltammetry behavior of DICP PtRuIr/C and DICP PtRu/C catalysts at low potential region. Scanning rate: 20 mV/s.

is very difficult for alloy formation even in binary catalysts. More intensive studies are needed to attain reliable conclusion. Some techniques, such as X-ray spectroscopy (XAS) and temperature-programmed reduction (TPR)/microcalorimetry of adsorbed CO, may be useful for this investigation [41,42].

CO stripping voltammetry is commonly used to test the activity of a catalyst for electrochemically oxidizing adsorbed CO on the catalyst. Fig. 4a shows the CO stripping voltammograms of the DICP PtRuIr/C, DICP PtRu/C, and E-TEK PtRu/C catalysts in 0.5 M H_2SO_4 at 25 °C after full adsorption of CO and subsequent purging of the solution with high-purity N_2. The figure also shows the second sweeping voltammograms. It should be noted that, due to the different microstructures and macrostructures of various electrocatalysts related to the different compositions and the synthesis routes, the current in the cyclic voltammetry measurements is usually normalized by the metal loadings (viz., mA/mg_{metal}) to compare the catalytic activity of the different electrocatalysts [9]. Therefore, all of the currents in our CO stripping voltammetry measurements are normalized per milligram of total metal.

It can be seen in Fig. 4a that adsorbed CO has been oxidized completely in a single scan, and no CO oxidation is monitored during the second scan for all three catalysts. The peak potential for CO_{ads} electro-oxidation on DICP PtRuIr/C, E-TEK PtRu/C, and DICP PtRu/C are 0.25, 0.31, and 0.45 V versus SCE, respectively, indicating that addition of Ir in the PtRu system leads to an enhanced activity for CO_{ads} oxidation, even higher than that for the commercial PtRu/C catalyst. Fig. 4b reveals the voltammetry behavior of DICP PtRuIr/C and DICP PtRu/C catalysts at low potential region, showing that the DICP PtRuIr/C catalyst exhibits a hydrogen oxidation peak in the hydride region ($-0.192 \rightarrow -0.158$ V vs. SCE) compared with DICP PtRu/C [38]. This is the result of hydrogen electro-oxidation via transient holes in the CO adlayer on metal active sites of DICP PtRuIr/C, implying the different surface structures of the two catalysts [43].

Although normalization of the current by the metal loadings facilitates the comparison of the different catalysts and can represent the economic efficiency of the catalysts, the mass-current density does not take into account the number of surface active metal sites [9]. Usually, the electrochemically active surface (EAS) is used to reflect the intrinsic electrocatalytic activity, (i.e., the number of the active surface metal sites) of a catalyst [9]. The EAS of DICP PtRuIr/C, E-TEK PtRu/C, and DICP PtRu/C, calculated from the area of the corresponding electrocatalytic oxidation peak for CO_{ads} are 64.3, 49.2, and 30.6 m^2/g metal, respectively. These results further reveal that DICP PtRuIr/C has very high CO_{ads} electro-oxidation activity. It is interesting to note that DICP PtRuIr/C has not only a much lower peak potential for CO_{ads} oxidation, but also a higher EAS compared with those for DICP PtRu/C catalyst. Generally, the particle size can affect the EAS of an electrocatalyst [9]. As demonstrated by TEM and XRD, however, the particle size and size distribution of the DICP PtRuIr/C and DICP PtRu/C catalysts are close. Although smaller particles of DICP PtRuIr/C catalyst can contribute to some extent to more active metal sites for CO_{ads} electro-oxidation, we believe that such a small difference in particle size of the two catalysts should not produce a significant difference in the number of active sites.

Herein we suggest that this may be rationalized by recognizing two possibilities. One of these is that iridium may adsorb CO or that addition of, say, Ir in the PtRu system may increase the active metal sites for CO adsorption and electro-oxidation. Bearing this in mind, we prepared 40% Ir/C in the same way as for the DICP PtRuIr/C and DICP PtRu/C catalysts. The Ir content of the DICP Ir/C catalyst is given in Table 1. Figs. 5a and 5b show the TEM image and the histogram of the particle size distributions of DICP Ir/C catalyst, respectively. As it is shown in Fig. 5, the metal particles are uniformly dispersed on the support. The mean particle diameter is 3.0 nm and the size ranges between 1 and 7 nm, which are close to those of the DICP PtRuIr/C and the DICP PtRu/C catalysts. Fig. 6 shows the CO stripping voltammogram of DICP Ir/C catalyst. As can be seen in Fig. 6, the peak potential of CO_{ads} electro-oxidation for DICP Ir/C catalyst is 0.66 V versus SCE, which is 410 mV higher than that for DICP PtRuIr/C and 210 mV higher than that for DICP PtRu/C. Integration of the CO_{ads} stripping peak gives a 40.4 m^2/g metal of EAS. The EAS for the DICP PtRuIr/C catalyst approximates to the summation of the values of DICP PtRu/C and DICP Ir/C catalysts. This may support the above-mentioned supposition that inclusion of Ir in the PtRu system could increase the active metal sites for CO adsorption and electro-oxidation. The much lower peak potential for CO oxidation on DICP PtRuIr/C with respect to DICP PtRu/C and

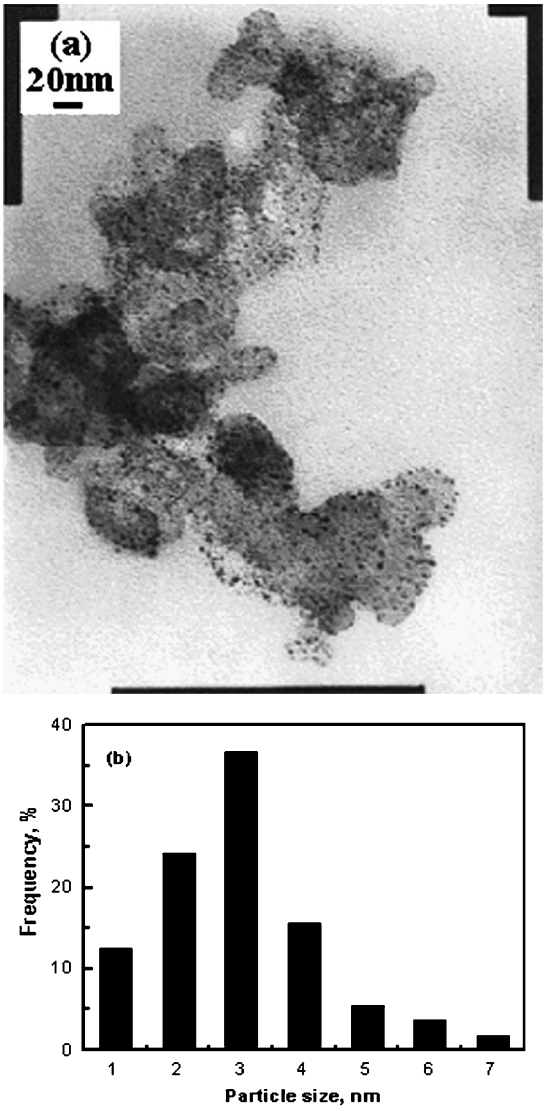

Fig. 5. (a) Bright-field TEM image and (b) the histogram of metal particles diameters of DICP Ir/C catalyst.

DICP Ir/C is attributed to the interaction between the species on the catalyst surface (vide infra). Moreover, the low EAS of the DICP PtRu/C catalyst may also arise from the formation of an improper alloy [9].

It is surprising that DICP PtRu/C catalyst, although prepared by the same way as that for DICP PtRuIr/C catalyst, exhibits much lower activity for CO_{ads} electro-oxidation. This could be presumably ascribed to its surface structure associated with the nonoptimum synthesis conditions [9,13,41].

Fig. 7 shows the polarization curves with all of the current densities normalized per cm^2 of active area of the MEAs. As indicated in Fig. 7, the DICP PtRuIr/C catalyst outperforms both the DICP PtRu/C catalyst and the E-TEK PtRu/C catalyst at all recorded current densities. For example, at a current density of 100 mA/cm^2, the voltage for DICP PtRuIr/C is 0.864 V, which is 50 mV higher that for DICP PtRu/C and 35 mV higher than that for E-TEK PtRu/C. The performance results of the catalysts in the single cells are in good agreement with those in CO stripping voltammetry measurements.

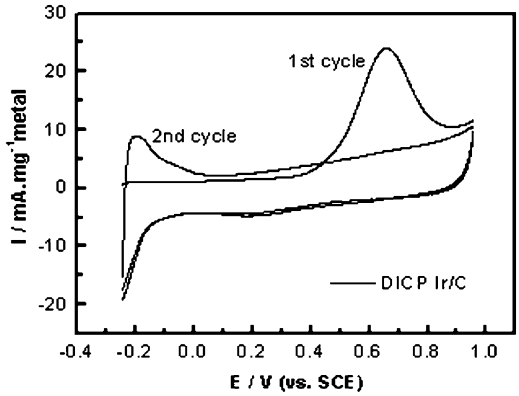

Fig. 6. CO-stripping voltammogram of DICP Ir/C catalyst in 0.5 M H_2SO_4 at 25 °C. Scanning rate: 20 mV/s.

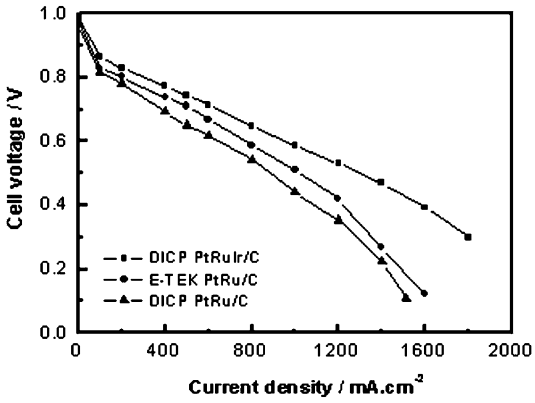

Fig. 7. PEM fuel cell polarization curves comparing DICP PtRuIr/C and DICP PtRu/C as the anode catalysts with the commercial E-TEK 40 wt% PtRu/C catalyst. Anode catalyst powder loading: 1 mg/cm^2. Cathode: the commercial Johnson Matthey 50 wt% Pt/C catalyst with platinum loading of 0.37 mg/cm^2. Cell temperature: 80 °C. Fuel gas: 100 ppm CO/H_2 (0.2 MPa), oxidant: O_2 (0.2 MPa). The fuel gas and the oxidant are humidified at 90 and 85 °C, respectively, before feeding into the cell. The MEAs have an active area of 5 cm^2.

Analyses of inlet and outlet anode gases of the cells were carried out by means of gas chromatography. Mass balance calculations showed that ca. 70, 46, and 55% of carbon monoxide were converted to carbon dioxide for the DICP PtRuIr/C, DICP PtRu/C and E-TEK PtRu/C catalysts, respectively, at 100 mA/cm^2, indicating that the promoted mechanism occurs on these catalysts. The trend of the analyses appears to be the same as those in the CO stripping voltammetry measurements and in the single-cell tests.

To shed more light on the nature of excellent CO-tolerant performance of our DICP PtRuIr/C nanocomposite (i.e., to understand the factors causing the enhancement in CO_{ads} electro-oxidation activity), we performed XPS analyses of DICP PtRuIr/C and DICP PtRu/C catalysts to determine the oxidation states of the metals on the catalyst surface. It should be noted that the particle size of the two catalysts (~3 nm) is in the range of XPS scrutiny [17,23]. Because the Ru3d region overlays with the C1s region, the less-intense Ru3p region was thus analyzed. The deconvolution of the Pt4f core-level region was carried out by referring to the literature sources [9,14,16, 22–24,27,34,44], while the Ru3p and Ir4f regions are deconvo-

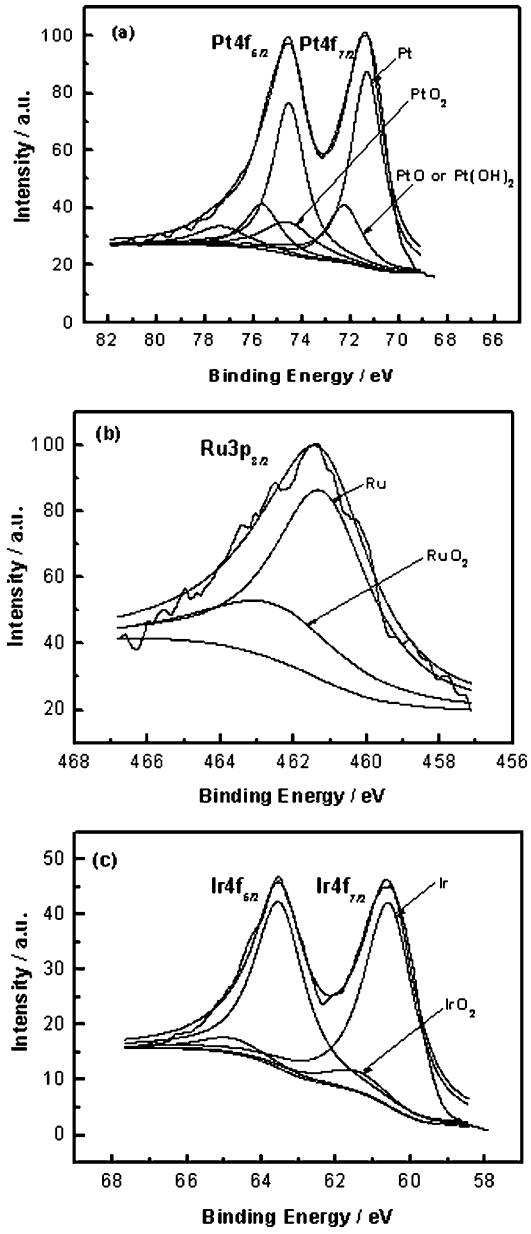

Fig. 8. XPS core level spectra for Pt4f (a), $Ru3p_{3/2}$ (b) and Ir 4f (c) photoemission from DICP PtRuIr/C catalyst.

luted according to [9,10,14,16,23,24,27,44] and [27,38,44,45], respectively.

Figs. 8a–8c show the XPS spectra for Pt4f, $Ru3p_{3/2}$, and Ir4f core-level regions of the DICP PtRuIr/C catalyst. Deconvolution of the Pt4f region shows the presence of three pairs of doublets. The most intense doublet with binding energies of 71.3 eV ($Pt4f_{7/2}$) and 74.5 eV ($Pt4f_{5/2}$) was attributed to metallic Pt. Peaks at 72.2 and 75.6 eV could be assigned to Pt^{2+} as in either PtO or $Pt(OH)_2$. The third doublet found at 74.5 and 77.3 eV appears to be Pt^{4+}, possibly as PtO_2; 64.6% of the platinum exists as metallic Pt, 20.3% exists as PtO or $Pt(OH)_2$, and 15.1% exists as PtO_2. The $Ru3p_{3/2}$ spectrum was deconvoluted into two peaks at 461.2 and 462.5 eV, which correspond to metallic Ru and RuO_2; 70.3% of the Ru exists as metallic Ru, and 29.7% exists as RuO_2. The most intense Ir4f peak of

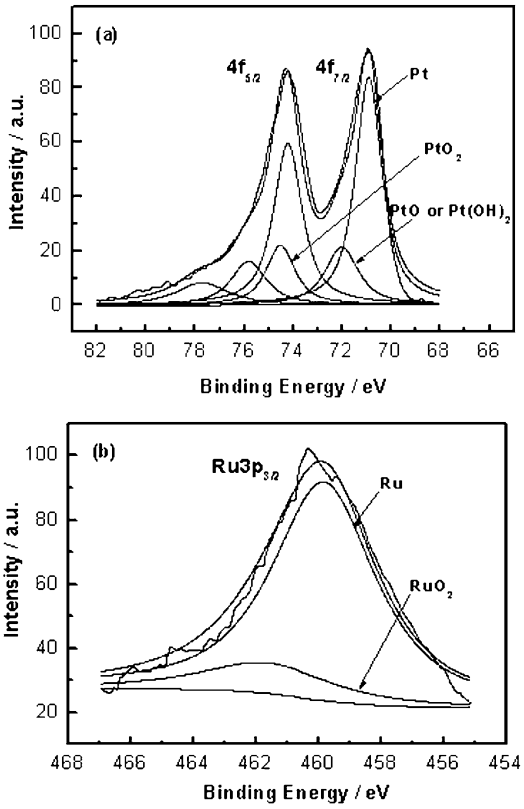

Fig. 9. XPS core level spectra for Pt 4f (a) and $Ru3p_{3/2}$ (b) photoemission from DICP PtRu/C catalyst.

the DICP PtRuIr/C catalyst lies near the Pt4f satellites. After these satellites were removed, a resolved signal was discerned. Deconvolution of the signal showed the presence of two doublets. Comparison of the observed binding energies with those reported in the literature suggests that the two species are metallic Ir and IrO_2. The deconvolution results suggest that 89% of the iridium is present as the metal state and 11% is present as the oxidized state.

Figs. 9a–9b show the XPS spectra for Pt4f and $Ru3p_{3/2}$ regions of the DICP PtRu/C catalyst. Like those for the DICP PtRuIr/C catalyst, here the Pt4f signal is also deconvoluted into three pairs of doublets attributed to metallic Pt, Pt^{2+}, and PtO_2. Platinum in the DICP PtRu/C catalyst is also predominantly in the metallic state (69.8%). The PtO [or $Pt(OH)_2$] and PtO_2 account for 15.7 and 15.5%, respectively. The $Ru3p_{3/2}$ spectrum consists of 84.6% metallic Ru and 15.4% RuO_2.

It is noteworthy that no chloride was detected by XPS for the two catalysts. This finding indicates the complete removal of this detrimental species.

Up to now, we have compared the as-prepared DICP PtRuIr/C and DICP PtRu/C catalysts in terms of metal particle morphology, particle size, size distribution, compositional homogeneity, phase information and surface metal oxidation state, and other factors. It appears that the enhanced performance of the DICP PtRuIr/C catalyst should be ascribed mainly to the iridium additives.

Previous studies have established that the IrO_2 has good electronic conductivity and high electrocatalytic activity toward

oxygen evolution in acid medium [27–30]. Our gas chromatography analysis has shown that much more carbon monoxide is oxidized on the DICP PtRuIr/C catalyst than on the two PtRu/C analogues (vide ante). Therefore, we believe that iridium additives, at least IrO_2, serve as cocatalysts for electro-oxidation of CO chemisorbed on Pt, hence releasing more active Pt sites for HOR. Contribution of metallic Ir to CO_{ads} electro-oxidation should not be ruled out for the moment, and more intensive investigation is needed.

As mentioned above, the particle sizes of both the DICP PtRuIr/C and DICP PtRu/C catalysts are within the range of XPS scrutiny. Based on the relative concentrations of the surface species and the bulk content of the metals (see Table 1) in the two as-prepared catalysts, RuO_2 accounts for ca. 1.5% in DICP PtRuIr/C and 1.6% in DICP PtRu/C. It is interesting that although RuO_2 has a higher activity for the oxygen evolution reaction than IrO_2 [29] and the RuO_2 content is slightly higher in the DICP PtRu/C catalyst, it has a much lower activity for CO_{ads} electro-oxidation than that of the DICP PtRuIr/C catalyst, as indicated by CO stripping voltammetry and single-cell measurements. The RuO_2–IrO_2 interaction may play a beneficial role and facilitate elimination of CO_{ads} from the active Pt sites. Gasteiger et al. [15] demonstrated the ability of Ru surface atoms to provide nucleation sites for oxygen-containing species (e.g., hydroxyl group) at lower potentials than that for Pt. Kötz and Stucki [29] reported a higher affinity of oxygen for Ru than that for Ir.

We suggest that the excellent performance of our DICP PtRuIr/C catalyst can be attributed to the facile electro-oxidation of CO_{ads} promoted by iridium additives. It is supposed that in our PtRuIr system, RuO_2–IrO_2 interaction promotes the formation of hydroxyl species by dissociating water at a lower potential with respect to the PtRu system. Moreover, this interaction could also weaken the bonding between the hydroxyl species and the catalyst surface as compared with the bonding on PtRu nanoparticles. The more weakly adsorbed hydroxyl species further promotes electro-oxidation of CO_{ads} on the active metal sites at a lower potential, thus improving the performance. Although this mechanism appears to be rather speculative, it may be of relevance in explaining the excellent catalytic activity of our PtRuIr/C catalyst for HOR in the presence of carbon monoxide.

It has been established that the stability of RuO_2 in acid media is significantly improved by admixture of IrO_2 [29,30]. Thus, the inclusion of Ir in the PtRu system may be advantageous to the long-term stability of PEM fuel cells. However, because the issue of electrocatalyst stability is critical and complicated [24], more intensive investigation is warranted.

It should be noted that alloying with some other metals can make platinum less reactive to carbon monoxide [3,6]; that is, the Pt–CO_{ads} bond is weakened or CO_{ads} coverage is reduced [42], as postulated by the intrinsic mechanism (vide ante). The weakened Pt–CO_{ads} bond can also contribute to the facilitation of CO_{ads} oxidation. This may occur in our DICP PtRuIr/C catalyst. However, as discussed in XRD section, the formation of ternary alloy for the DICP PtRuIr/C catalyst is far from conclusive at this stage; whether there is an intrinsic mechanism in this catalyst merits detailed investigation.

4. Conclusion

In summary, a carbon-supported PtRuIr catalyst was synthesized via the MIPA strategy. The PtRuIr/C catalyst displayed greatly enhanced activity for CO_{ads} electro-oxidation, even higher than that of the commercial E-TEK PtRu/C catalyst. Characterizations showed that the superior performance of the PtRuIr/C catalyst should result from the iridium additives, particularly IrO_2. A speculative mechanism associated with the excellent performance of PtRuIr/C is proposed. It is supposed that the superior activity for CO_{ads} electro-oxidation of the catalyst should be attributed mainly to the interaction between RuO_2 and IrO_2. We believe that the excellent electrocatalytic activity of our carbon-supported PtRuIr nanocomposite for HOR in the presence of CO is encouraging for the research and development of PEM fuel cells. Further refinement of the preparative conditions will hopefully afford even better catalyst performance.

Acknowledgments

The financial support of the National Natural Science Foundation of China (grants 50236010 and 20206030) is appreciated.

References

[1] P. Costamagna, S. Srinivasan, J. Power Sources 102 (2001) 242.
[2] G. Hoogers, D. Thomposett, CATTECH 3 (1999) 106.
[3] E. Antolini, Mater. Chem. Phys. 78 (2003) 563.
[4] E. Antolini, J. Appl. Electrochem. 34 (2004) 563.
[5] P.K. Babu, H.S. Kim, E. Oldfield, A. Wieckowski, J. Phys. Chem. B 107 (2003) 7595.
[6] E. Christoffersen, P. Liu, A. Ruban, H.L. Skriver, J.K. Nørskov, J. Catal. 199 (2001) 123.
[7] J.J. Baschuk, X. Li, Int. J. Energy Res. 25 (2001) 695.
[8] T.J. Schmidt, M. Noeske, H.A. Gasteiger, R.J. Behm, P. Britz, W. Brijoux, H. Bönnemann, Langmuir 13 (1997) 2591.
[9] Y. Takasu, T. Fujiwara, Y. Murakami, K. Sasaki, M. Oguri, T. Asaki, W. Sugimoto, J. Electrochem. Soc. 147 (2000) 4421.
[10] D.L. Boxall, G.A. Deluga, E.A. Kenik, W.D. King, C.M. Lukehart, Chem. Mater. 13 (2001) 891.
[11] Y.M. Liang, H.M. Zhang, B.L. Yi, Z.H. Zhang, Z.C. Tan, Carbon 43 (2005) 3144.
[12] C. Lu, R.I. Masel, J. Phys. Chem. B 105 (2001) 9793.
[13] V. Radmilović, H.A. Gasteiger, P.N. Ross Jr., J. Catal. 154 (1995) 98.
[14] C. Bock, C. Paquet, M. Couillard, G.A. Botton, B.R. MacDougall, J. Am. Chem. Soc. 126 (2004) 8028.
[15] H.A. Gasteiger, N. Marković, P.N. Ross Jr., E.J. Cairns, J. Phys. Chem. 98 (1994) 617.
[16] B. Yang, Q. Lu, Y. Wang, L. Zhuang, J. Lu, P. Liu, J. Wang, R. Wang, Chem. Mater. 15 (2003) 3552.
[17] G.A. Camara, M.J. Giz, V.A. Paganin, E.A. Ticianelli, J. Electroanal. Chem. 537 (2002) 21.
[18] G. Samjeské, H. Wang, T. Löffler, H. Baltruschat, Electrochim. Acta 47 (2002) 3681.
[19] M. Götz, H. Wendt, Electrochim. Acta 43 (1998) 3637.
[20] P. Shen, K. Chen, A.C.C. Tseung, J. Electrochem. Soc. 142 (1995) L85.
[21] D.C. Papageorgopoulos, M. Keijzer, F.A. de Bruijn, Electrochim. Acta 48 (2002) 197.

[22] T.C. Deivaraj, W. Chen, J.Y. Lee, J. Mater. Chem. 13 (2003) 2555.
[23] K.W. Park, J.H. Choi, B.K. Kwon, S.A. Lee, Y.E. Sung, H.Y. Ha, S.A. Hong, H. Kim, A. Wieckowski, J. Phys. Chem. B 106 (2002) 1869.
[24] K.W. Park, J.H. Choi, B.K. Kwon, S.A. Lee, C. Pak, H. Chang, Y.E. Sung, J. Catal. 224 (2004) 236.
[25] H.R. Colón-Mercado, H. Kim, B.N. Popov, Electrochem. Commun. 6 (2004) 759.
[26] T.J. Schmidt, Z. Jusys, H.A. Gasteiger, R.J. Behm, U. Endruschat, H. Bönnemann, J. Electroanal. Chem. 501 (2001) 132.
[27] Y.Y. Dai, Z.T. Liu, Q.Z. Jiang, D.Y. Zhang, Z.F. Ma, Chin. J. Nonferrous Metals 14 (2004) 402.
[28] A. Chen, D.J. La Russa, B. Miller, Langmuir 20 (2004) 9695.
[29] R. Kötz, S. Stucki, Electrochim. Acta 31 (1986) 1311.
[30] L.A. da Silva, V.A. Alves, M.A.P. da Silva, S. Trasatti, J.F.C. Boodts, Electrochim. Acta 42 (1997) 271.
[31] D.R. Lide (Ed.), Handbook of Chemistry and Physics, eightieth ed., CRC Press LLC, New York, 1999, p. 148, chap. 6.
[32] S. Komarneni, R. Pidugu, Q.H. Li, R. Roy, J. Mater. Res. 10 (1995) 1687.
[33] X. Li, W.X. Chen, J. Zhao, W. Xing, Z.D. Xu, Carbon 43 (2005) 2168.
[34] Z. Liu, L.M. Gan, L. Hong, W. Chen, J.Y. Lee, J. Power Sources 139 (2005) 73.
[35] K.Y. Chan, J. Ding, J. Ren, S. Cheng, K.Y. Tsang, J. Mater. Chem. 14 (2004) 505.
[36] R. Harpeness, A. Gedanken, Langmuir 20 (2004) 3431.
[37] I. Dobrosz, K. Jiratova, V. Pitchon, J.M. Rynkowski, J. Mol. Catal. A: Chem. 234 (2005) 187.
[38] Y. Verde, G. Alonso-Nunez, M. Miki-Yoshida, M. José-Yacamán, V.H. Ramos, A. Keer, Catal. Today 107–108 (2005) 826.
[39] T. Kobayashi, A. Ueda, Y. Yamada, H. Shioyama, Appl. Surf. Sci. 223 (2004) 102.
[40] B.L. Gratiet, H. Remita, G. Picq, M.O. Delcourt, J. Catal. 164 (1996) 36.
[41] D.G. Liu, J.F. Lee, M.T. Tang, J. Mol. Catal. A: Chem. 240 (2005) 197.
[42] Y.J. Zhang, A. Maroto-Valiente, I. Rodriguez-Ramos, Q. Xin, A. Guerrero-Ruiz, Catal. Today 93–95 (2004) 619.
[43] H.A. Gasteiger, N.M. Marković, P.N. Ross Jr., J. Phys. Chem. 99 (1995) 16757.
[44] A. Hamnett, B.J. Kennedy, Electrochim. Acta 33 (1988) 1613.
[45] J.L. Zang, G.X. Xiong, Chin. J. Catal. 1 (1980) 73.